A&A 490, 893–904 (2008)
DOI: 10.1051/0004-6361:20079299

Astronomy & Astrophysics

Radio-loud AGN in the XMM-LSS field

II. A dichotomy in environment and accretion mode?

C. Tasse[1], P. N. Best[2], H. Röttgering[1], and D. Le Borgne[3]

[1] Leiden Observatory, University of Leiden, PO Box 9513, 2300 RA Leiden, The Netherlands
e-mail: tasse@strw.leidenuniv.nl
[2] SUPA, Institute for Astronomy, Royal Observatory Edinburgh, Blackford Hill, Edinburgh EH9 3HJ, UK
[3] CEA/DSM/DAPNIA, Service d'Astrophysique, Saclay, 91191 Gif-sur-Yvette, France

Received 20 December 2007 / Accepted 9 May 2008

ABSTRACT

In recent years, several authors have argued that low luminosity radio-loud active galactic nuclei (AGN) have a different mode of accretion, triggered by different physical mechanisms, than "normal" optically- or X-ray-selected AGN. The latter have a radiatively efficient nucleus (sometimes called "Quasar-mode"), which according to the unified scheme may be obscured from direct view at optical wavelengths, whereas essentially all of the energetic output of the low-luminosity radio-loud AGN is in their radio jets ("Radio-mode").

In this paper, we independently study the internal and environmental properties of the optical hosts of the sample of ∼110 radio sources with redshifts $0.1 < z < 1.2$ in the XMM-LSS Survey region. We do this by building a comoving-scale-dependent overdensity parameter, based on the photometric redshift probability functions, to constrain the small (∼75 kpc) and large (∼450 kpc) scale environments of radio sources independently from their stellar mass estimates. Our results support the picture in which the comoving evolution of radio sources in the redshift range $\lesssim 1$ is caused by two distinct galaxy populations, whose radio source activity is triggered by two different mechanisms. The first population, which dominates at high stellar masses ($M > 10^{10.5-10.8}\ M_{\odot}$) is that of massive elliptical galaxies, lying in galaxy groups or clusters, where the radio source is triggered by the cooling of the hot gas in their atmosphere. At these stellar masses, we find that the fraction of galaxies that host radio-loud AGN is essentially the same as that in the local Universe. The second population of radio sources have lower stellar masses, lie in large scale underdensities, and show excess mid-IR emission consistent with a hidden radiatively efficient active nucleus. The radio-loud fraction at these masses is increased relative to the local Universe. We argue that galaxy mergers and interactions may play an important role in triggering the AGN activity of this second population.

Key words. surveys – galaxies: active – galaxies: fundamental parameters – radio continuum: galaxies – infrared: galaxies – cosmology: large-scale structure of Universe

1. Introduction

Active galactic nuclei (AGN) have regained attention in the last decade since they are thought to play a major role in the process of galaxy formation. During their short lifetime, the enormous amount of energy they produce in the form of ionising radiation or relativistic jets can have a significant effect on their small-scale (internal) and large scale (external) surroundings. It appears from semi-analytical models and high resolution numerical simulations that the AGN energetic feedback is a vital ingredient for reproducing some of the observed features of the Universe, such as the stellar galaxy mass function (Croton et al. 2005; Best et al. 2006), or the black hole mass versus bulge mass relationship (Gebhardt et al. 2000; Springel et al. 2005a).

Unified schemes give a good description of the observed properties of radio-quiet AGN (e.g. Elitzur 2007). In this picture, the nuclear activity is produced by matter accreted onto a supermassive black hole, with an optically thick dusty torus surrounding the nucleus such that from some directions the AGN is seen directly while from others it can be obscured. The most powerful radio sources also follow the unified scheme, but there is a subset of radio loud AGN (especially at low radio power) for which the unified scheme does not seem appropriate: these sources lack infrared emission from the dusty torus (Whysong & Antonucci 2004; Ogle et al. 2006), as well as luminous emission lines (Hine & Longair 1979; Laing et al. 1994; Jackson & Rawlings 1997) and accretion related X-ray emission (Hardcastle et al. 2006; Evans et al. 2006). These observations are supported by recent results from large surveys (Best et al. 2005) indicating that the low-luminosity radio-loud AGN and the radio-quiet (optical) AGN phenomena are statistically independent. Many authors have argued that the low luminosity radio-loud and the optically active AGN correspond to two different accretion modes (the "Radio mode" or "Hot mode" versus the "Quasar mode" or "Cold mode"; for a discussion see Croton et al. 2006; Hardcastle et al. 2007). In this picture, the quasar mode is radiatively efficient, and is caused by accretion of cold gas onto the supermassive black hole, while the radio mode results from the accretion of hot gas and is radiatively inefficient. As we show in this paper, the nature of the processes that trigger the black hole activity might be important in giving rise to these two AGN modes.

It has often been proposed that galaxy mergers and interactions both trigger a starburst and fuel the central super-massive black hole. Although the situation remains controversial for the

low luminosity optically active AGN (Veilleux 2003; Schmitt 2004), observations of large samples of optically-selected AGN from the Sloan Digital Sky Survey show clear evidence that the luminous optically active AGN are associated with young stellar populations (Kauffmann et al. 2003). At the extreme end, this scenario is supported by observations of ultra-luminous infrared galaxies (ULIRGs, Sanders & Mirabel 1996), that are in general associated with galaxy mergers, and have bolometric luminosities similar to quasars (Sanders et al. 1988a); some ULIRGs are known to hide a buried AGN in their nucleus (e.g. Sanders et al. 1988b). High resolution numerical simulations (Springel et al. 2005a,b) have consistently shown that the AGN activity remains obscured during most of the starburst and AGN activity phase.

In contrast to this, low-luminosity radio-loud AGN in the nearby Universe are seen to be preferentially hosted by massive elliptical galaxies, which tend to be found in richer, cold-gas poor environments, where gas-rich galaxy mergers are less likely to occur. The cooling of the hot X-ray emitting gas observed in the atmospheres of massive elliptical galaxies (Mathews & Brighenti 2003) has been proposed as an alternative triggering process for the AGN activity in these sources. Based on a large sample of radio sources in the SDSS, Best et al. (2005) argued that the gas cooling rate has the same dependence on stellar mass as the fraction of low luminosity radio-loud galaxies. This suggests that the gas that has radiatively cooled from the X-ray emitting atmosphere may trigger the AGN activity.

In this paper, we study the properties of a well-controlled sample of ∼110 radio loud AGN situated at $z \lesssim 1.2$, to place constraints on the triggering mechanisms, and the evolution of the radio-loud AGN population. Our results support the picture in which galaxy mergers and gas cooling from the hot atmosphere of massive ellipticals compete to trigger the quasar and the radio mode respectively (Hardcastle et al. 2007). The evolution of these two processes through cosmic time might play an important role in the evolution of the radio luminosity function.

In Sect. 2, we present the sample, and its associated parameters. In Sect. 3, we derive a radio loud fraction ($f_{\rm RL}$) versus stellar mass relation equivalent to that which has been estimated at low redshift in the SDSS (Best et al. 2005). In Sect. 4, we construct a scale dependent overdensity parameter that allows us to study the environment of radio sources independently from their intrinsic properties estimates. We discuss the results in Sect. 5.

2. A sample of radio selected AGN in the XMM-LSS field

In this section we briefly introduce the XMM-LSS survey, and the sample of radio sources that has been described in full detail in Tasse et al. (2008).

The XMM-Large Scale Structure field (XMM-LSS) is a 10 square degree extragalactic window observed by the XMM-Newton X-ray satellite in the 0.1–10 keV energy band. The XMM-LSS area has been followed up with a broad range of extragalactic surveys. The Wide-1 component of the Canada France Hawaï Telescope Legacy Survey (CFHTLS-W1) will image 7×7 deg^2 in the 5 broad band $u^*g'r'i'z'$ filters, reaching an i-band magnitude limit of $i_{\rm AB} \sim 25$. As part of the Spitzer Wide-area InfraRed Extragalactic legacy survey (SWIRE, Lonsdale et al. 2003), the XMM-LSS field was imaged in 7 infrared bands from 3.6 to 160 μm over ∼9 deg^2 (see Pierre et al. 2004, for a layout of the associated surveys). Low frequency radio surveys of the XMM-LSS field have been carried out with the Very Large Array (Tasse et al. 2006) at 74 and 325 MHz, and with the Giant Meterwave Radio Telescope (GMRT) at 230 and 610 MHz (Tasse et al. 2007).

In Tasse et al. (2008) we derived estimates of photometric redshifts, stellar masses (M), and specific star formation rates $\mathrm{sSFR}_{0.5}$ (averaged over the last 0.5 Gyr) for $\sim 3 \times 10^6$ galaxies in the CFHTLS-W1 field, using the ZPEG photometric redshift code (Le Borgne & Rocca-Volmerange 2002).

We matched the radio sources detected at 230, 325, and 610 MHz (Tasse et al. 2006, 2007) with their optical counterpart using the CFHTLS optical images. To do this we used a modified version of the likelihood ratio method described in great detail in Sutherland & Saunders (1992), which allowed us to derive for each radio source i, a probability $P^i_{\rm id}(j)$ of association with a given optical candidate j. Using Monte-Carlo simulations, we quantified and corrected for the contamination from misidentifications. Each optical candidate was also cross-identified with infrared SWIRE sources at 3.6, 4.5, 5.8, 8.0 and 24 μm. From the redshift and spectral index estimates[1], we derived the 1.4 GHz radio power of each radio source host.

In order to select a subsample of objects having reliable photometric redshift estimates, we applied a few basic cuts to the identified sample, rejecting masked, saturated, and point-like objects. Furthermore, the objects that did not satisfy the following properties were rejected:

- $18 < i < 24$
- $N_{\rm b} \geq 3$
- $0.1 < z_{\rm ph} < 1.2$

where $N_{\rm b}$ is the number of bands in which the object is detected, and $z_{\rm ph}$ is the photometric redshift estimate.

In this paper, we reject the objects classified as type-1 AGN in Tasse et al. (2008), since those have corrupted physical parameter estimates (∼12.6% of the sample). This selection is unlikely to affect the results presented in this paper (see the discussion in Sect. 3.1). Since our goal is the study of the properties and environment of radio-loud AGN, we also reject starburst galaxies (∼3.3% of the sample). The uncertainties associated with the selected sample of radio-loud AGN are typically $\sigma(z) \sim 0.1$, $\sigma(\log(M/[M_\odot])) \sim 0.15$ and $\sigma(\log(sSFR_{0.5}/[\mathrm{yr}^{-1}])) \sim 0.3$ (Tasse et al. 2008). As shown in Fig. 1, the selected sample should contain both FRI-type and FRII-type radio sources: below the radio power cut of $P^{\rm cut}_{1.4} = 10^{25}$ W/Hz, most radio sources are edge-darkened FRIs, while the more luminous sources are mostly edge-brightened FRIIs (for a discussion see Snellen & Best 2001).

3. Intrinsic properties of the host galaxies of radio sources

In this section, we study the intrinsic properties of the host galaxies of the radio source sample described above. Specifically, in Sect. 3.1 we compare their stellar mass function to that of the normal galaxies in different redshift bin and in Sect. 3.2 we address the evolution of radio sources using the $V/V_{\rm max}$ estimator. In Sect. 3.3, we compute an infrared excess estimator.

[1] The spectral index of each radio source was estimated by fitting a power-law to the flux density measurement available at 74, 240, 325, 610 and 1400 MHz (Tasse et al. 2006, 2007; Condon et al. 1998). For the radio sources detected in only one band, we have assumed a spectral index $\alpha = -0.8$.

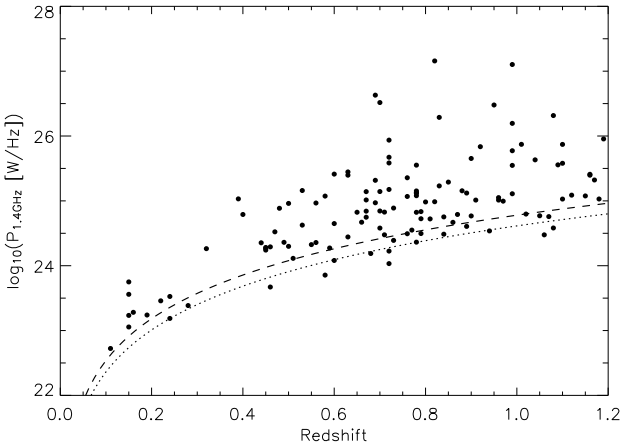

Fig. 1. The 1.4 GHz radio power of the selected radio sources (dots) as a function of their estimated redshift. The dashed and dotted lines show the completeness levels at 325 and 610 MHz respectively, as derived using the median flux density level of those surveys (5σ, Tasse et al. 2006, 2007), and assuming a spectral index $\alpha = -0.8$.

3.1. Stellar mass functions

We have derived the stellar mass function for normal galaxies ($\phi_{\rm Opt}$) in the redshift ranges $0.1 < z < 1.2$, $0.1 < z < 0.6$, $0.4 < z < 0.9$, and $0.7 < z < 1.2$, using the $1/V_{\rm max}$ estimator (Schmidt 1968; see Tasse et al. 2008, for details). In Fig. 2 we compare these mass functions with the mass functions derived for the host galaxies of the radio sources in the sample. As discussed in Tasse et al. (2008), our estimates of $\phi_{\rm Opt}$ (for all galaxies) are in good agreement over the full mass range with the stellar mass function as derived from the GOODS-MUSIC sample (Fontana et al. 2006); the low values obtained at low stellar masses in the higher redshift bin are discussed below. As expected from the SDSS-NVSS analysis (Best et al. 2005), the shape of $\phi_{\rm Rad}$ is different from $\phi_{\rm Opt}$, with the radio source host galaxies being biased towards more massive systems. Interestingly, while the comoving number density of normal galaxies decreases with redshift, the radio source host galaxies having $M < 10^{11}\ M_{\odot}$ show strong positive redshift evolution. In the redshift bin $0.7 < z < 1.2$, the stellar mass function is rather flat.

This effect is clearly shown in Fig. 3 which displays the fraction of galaxies that are radio-loud AGN ($f_{\rm RL} = \phi_{\rm Rad}/\phi_{\rm Opt}$), as a function of stellar mass in the four redshift bins. At low redshift and at $M \gtrsim 10^{10.5}\ M_{\odot}$, the shape and normalisation of our estimate of $f_{\rm RL}$ matches that found in the local Universe ($f_{\rm RL} \propto M^{2.5}$) by Best et al. (2005). However, we find evidence that the $f_{\rm RL} - M$ relation flattens at $M \lesssim 10^{10.5-11.0}\ M_{\odot}$. In the higher redshift bins the fraction of radio-loud objects agrees with the low redshift measurements for high stellar masses, but the lower stellar masses $M \lesssim 10^{10.5-11.0}$ show a strong evolution. The physical implications of these results are discussed in Sect. 5.

We investigate below the possibility that this effect is caused by (i) an incompleteness effect caused by our flux limited survey; (ii) the scatter along the stellar mass axis, due to the uncertainties in that parameter; and (iii) a selection effect due to the rejection of the type-1 AGN (Sect. 2).

Fontana et al. (2004) have extensively discussed a common incompleteness effect arising when computing comoving number densities from flux-limited surveys. The $1/V_{\rm max}$ estimator calculates the number densities by taking account of the differing detection limits of those galaxies *detected* in each given stellar mass bin. However, galaxies of a given stellar mass have different spectral types and may have very different mass-to-light ratios. Therefore, especially at high redshifts, galaxies of some spectral types may simply not be detected at all, and the $1/V_{\rm max}$ estimator will not correct for these, leading to an underestimation in the derived comoving number density. The host galaxies of radio sources may be significantly different from normal galaxies, hence may have mass-to-light ratios that differ on average to those of the normal galaxy population; this would lead to a different incompleteness for $\phi_{\rm Opt}$ and $\phi_{\rm Rad}$, thereby driving a bias in $f_{\rm RL}$. We investigate the possibility that this effect causes the flattening of the $f_{\rm RL} - M$ relation by estimating an upper limit to that bias. In the most extreme case, all radio source host galaxies are detected, but not all normal galaxies. The good match between our mass function for the normal galaxies and that of Fontana et al. (2006) indicates that this effect should not significantly affect $\phi_{\rm Opt}$ in the redshift bin $0.1 < z < 0.6$ and $0.4 < z < 0.9$. However, the lower estimate of the comoving number density for $M < 10^{10}\ M_{\odot}$ in the higher redshift bin indicates that the effect of incompleteness may affect our comoving number density estimate in that redshift range by a factor of $\sim$2. The bias in $f_{\rm RL}$ should therefore be less than a factor of $\sim$2, while the flattening involves differences of a factor of $\sim$100. We therefore conclude that this effect cannot explain the observed flattening.

We investigate the possibility that this flattening is produced by the uncertainty in the stellar masses estimate, that is higher at higher redshift. For this, we generate mass functions for the host galaxies of radio sources corresponding to a fraction $f_{\rm RL} = C_{11} M^{\alpha}$, where α is the slope of the relation and C_{11} is its normalisation at $10^{11}\ M_{\odot}$. We assume that the $V_{\rm max}$ within a given stellar mass bin will be similar for all galaxies of that bin. Given the average $V_{\rm max}$ of the objects of a given stellar mass, we estimate the true number of sources to be observed in a given stellar mass bin for each α. We then generate a simulated catalog corresponding to a $f_{\rm RL} \propto M^{\alpha}$ relation, by scattering the true stellar mass estimates: each object in a given stellar mass bin is given the stellar mass of the ith object of the S1 sample with a probability $p_i = P_{\rm id}(i) \times p_i(\Delta M)$, where $P_{\rm id}$ is the identification probability (Tasse et al. 2008) and $p_i(\Delta M)$ is the probability that the true stellar mass of object i is in the mass bin ΔM. The operation is repeated 10 times, and the fraction $f_{\rm RL}$ is re-evaluated in each mass bin. As expected the mass scatter has the effect of increasing the observed fraction of low stellar mass objects. We quantify this effect by calculating the χ^2 on a grid where the free parameters are α and C_{11}, and associated error bars are taken at $\chi^2_{\rm min} + 1$ (Avni & Bahcall 1976). Figure 4 shows the best fit parameters in different redshift slices. The normalisation C_{11} of $f_{\rm RL}$ stays roughly constant through redshift. At low redshift, the slope measurement gives a good fit to the $\alpha \sim 2.5$ found by Best et al. (2005), while it progressively flattens towards higher redshift, by only slightly less than the data. This shows that the effect of the stellar masses uncertainty cannot explain the flattening of the fraction-mass relation at low stellar masses.

As mentioned in Sect. 2, $\sim$12% of the radio-loud AGN were classified as type-1 (Tasse et al. 2008) and rejected. We discuss here the possible effect of this selection on our conclusions. If the stellar mass of the host galaxies of type-1 AGN are uniformly spread over all stellar masses, then the comoving number density and fraction in each stellar mass bin (Figs. 2 and 3) differ from their unbiased estimate by $\sim$12%. This difference is lower than the uncertainties on comoving number density and fraction

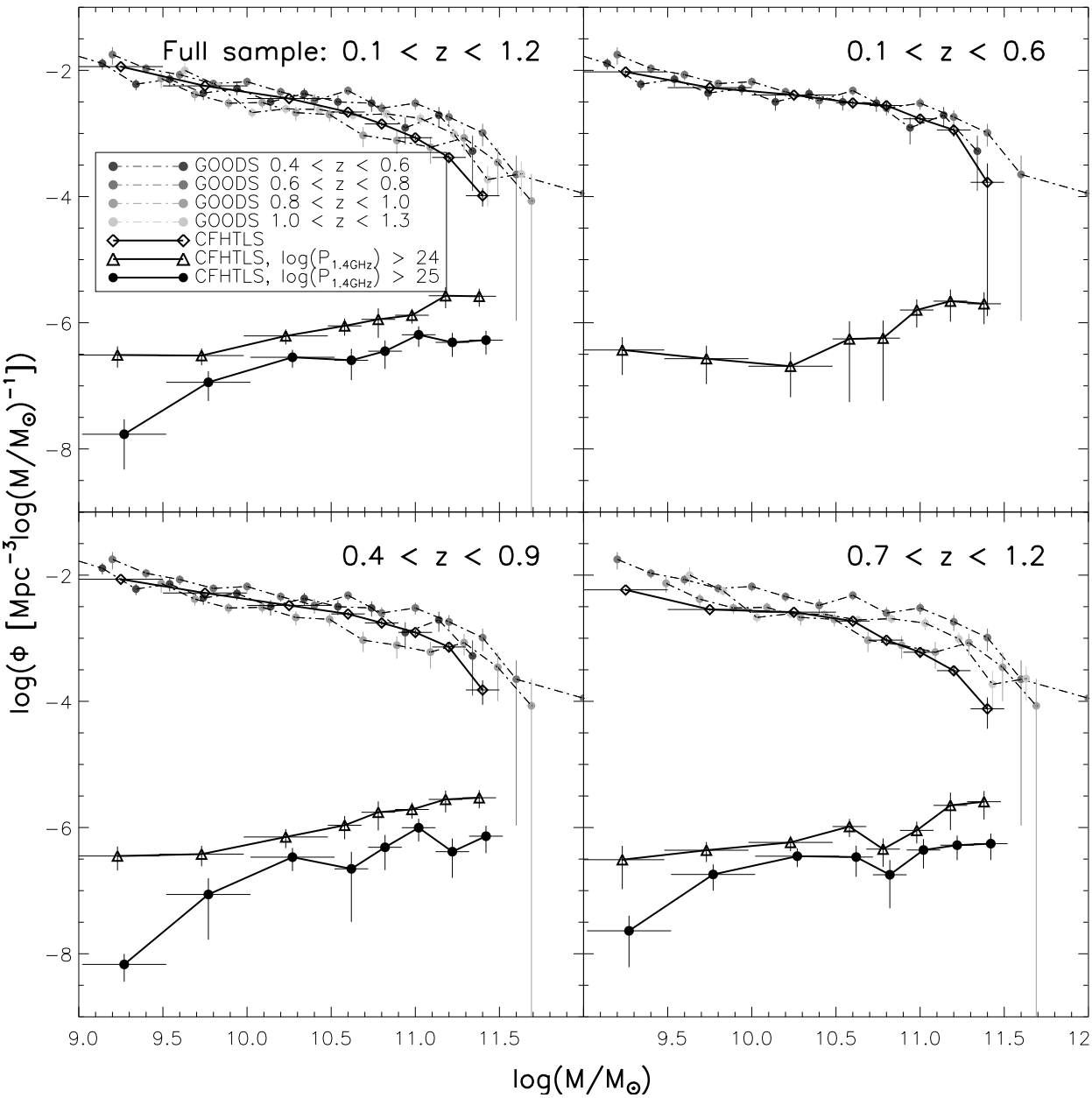

Fig. 2. Using the $1/V_{\rm max}$ comoving number density estimator, we have derived the stellar mass function for normal galaxies and for the host galaxies of radio sources in different redshift bins. For the normal galaxies, at all redshifts our estimate of the stellar mass function is in good agreement with its measurement in the GOODS surveys (Fontana et al. 2006), which suggests that the stellar masses estimates are reliable. The underestimation of the mass function at low stellar masses in the redshift bins $0.4 < z < 0.9$ and $0.7 < z < 1.2$ is due to incompleteness. The stellar mass function of the radio source host galaxies shows a very different, evolving shape.

estimates in all the stellar mass bin. If the type-1 AGN are biased towards a particular stellar mass this effect would be greater. However, in the extreme case where all the type-1 AGN are associated with the ∼12% galaxies that have the lowest stellar mass, the error in the results at low masses is a factor of 2, or 0.3 dex which is still within the estimated uncertainties. Therefore the bias introduced by the rejection of the type-1 AGN should not affect our conclusions.

3.2. Radio source evolution

In this section we address the issue of the evolution of radio source host galaxies within our sample using the $V/V_{\rm max}$ test (Schmidt 1968), where V is the comoving volume corresponding to the observed redshift of the radio source host galaxies, and $V_{\rm max}$ is the maximum available volume, described in Tasse et al. (2008). If the radio source population is not evolving, then $V/V_{\rm max}$ is uniformly distributed over the interval [0, 1] and $\langle V/V_{\rm max}\rangle = 0.5 \pm (12N)^{-0.5}$ where N is the number of sources in the sample (Avni & Bahcall 1980). Values of $\langle V/V_{\rm max}\rangle > 0.5$ imply a higher comoving number density at high redshifts, and therefore a negative evolution with cosmic time, whereas $\langle V/V_{\rm max}\rangle < 0.5$ indicates a positive evolution. A number of authors have used this estimator to address the cosmological evolution of radio sources selected at low frequency (Dunlop & Peacock 1990; Willott et al. 2001).

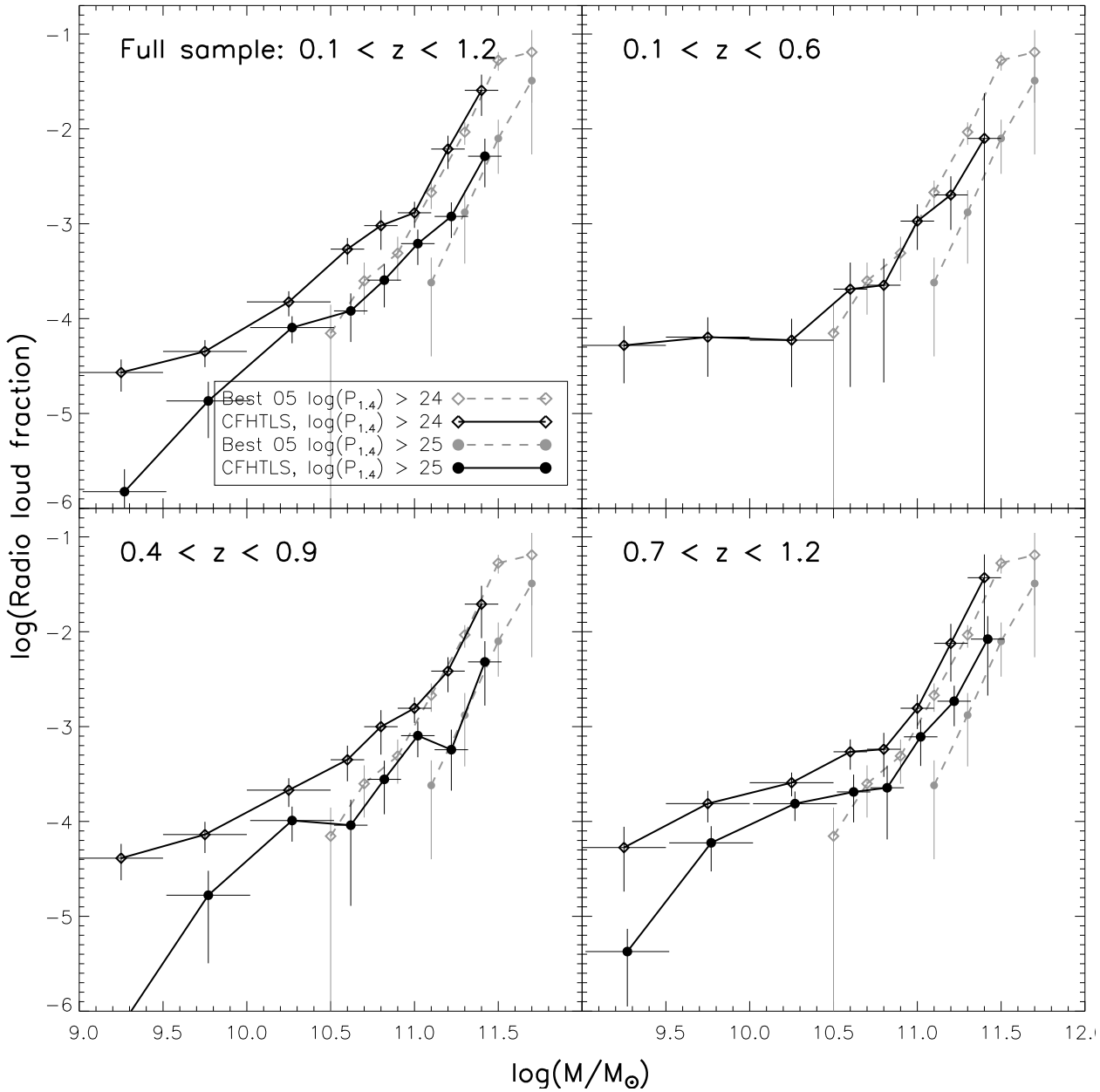

Fig. 3. The fraction of radio sources that are radio loud as a function of the stellar mass in a given comoving volume. These relations have been derived using the mass function estimates of the normal and radio loud galaxies presented in Fig. 2. In the lower redshift bins, our measurement of the $f_{\rm RL} - M$ relation matches its SDSS/NVSS $z \lesssim 0.3$ estimate (Best et al. 2005) both in normalisation and shape. While the fraction of high stellar mass objects $M \gtrsim 10^{11}\ M_{\odot}$ stays fairly constant with redshift, the fraction of lower stellar mass objects ($10^{10.0}\ M_{\odot} < M < 10^{10.5}\ M_{\odot}$) undergoes a strong evolution.

Figure 5 shows the comparison between the $\langle V/V_{\rm max}\rangle$ radio power relation for our sample and that of Clewley & Jarvis (2004), which was built from SDSS galaxies selected at 325 MHz. There is a good agreement between the two estimates.

In Fig. 6 we compute the $\langle V/V_{\rm max}\rangle$ in different stellar mass bins. Although radio sources are seen to evolve more than normal galaxies on average, their evolution shows a similar trend with stellar mass: low stellar mass systems evolve more than high stellar mass ones. These results are further discussed in Sect. 5.

3.3. Infrared properties of radio source host galaxies

As described in Tasse et al. (2008), we have associated with each radio source the infrared IRAC flux density measurements at 3.6, 4.5, 5.8 and 8.0 μm. Because ZPEG does not include infrared dust emission, the photometric redshifts have been computed from the magnitude measurements in the $u^*g'r'i'z'$ bands. We define an infrared excess parameter as:

$$\Delta_{\rm IR} = \log\left(F_{\nu}(\lambda_{\rm IRAC})/F_{\nu}^{\rm ZPEG}(\lambda_{\rm IRAC})\right) \quad (1)$$

where $F_{\nu}(\lambda_{\rm IRAC})$ is the IRAC flux density measurement at $\lambda_{\rm IRAC}$ and $F_{\nu}^{\rm ZPEG}(\lambda_{\rm IRAC})$ is the flux density measurement from the ZPEG best fit template at $\lambda_{\rm IRAC}$. The infrared excesses are computed in the observer frame.

Figure 7 shows the infrared excess at 3.6 μm computed for the normal galaxy population and for radio source host galaxies. The infrared excess is higher for the radio source host galaxies than for the normal galaxies, especially at low stellar masses. However, the radio sources host galaxies and the normal galaxy

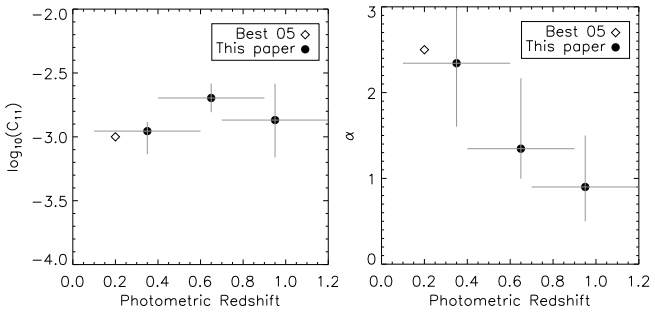

Fig. 4. This figure shows the best fit values for the parameters C_{11} (*left panel*) and α (*right panel*) in each redshift bin (see text). The low values of α in the higher redshift bins suggests that the scatter introduced by the stellar mass uncertainty cannot explain the flattening of the $f_{\rm RL} - M$ relation seen in Fig. 3.

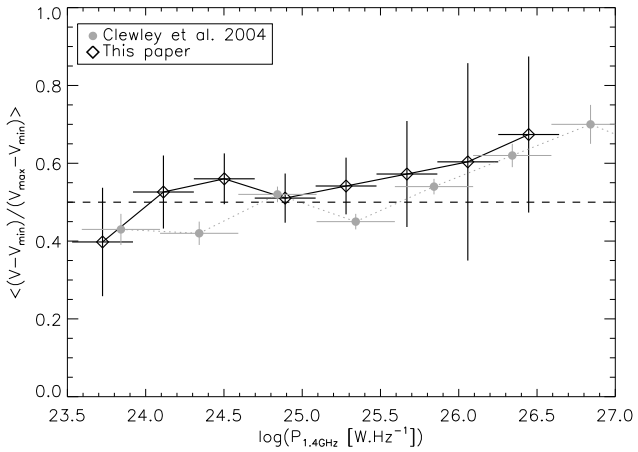

Fig. 5. The averaged $V/V_{\rm max}$ in different radio power ranges for our sample, as compared to the estimates of Clewley & Jarvis (2004).

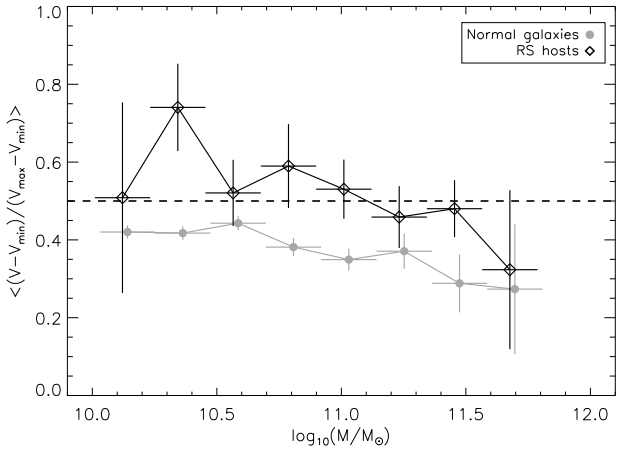

Fig. 6. The averaged $V/V_{\rm max}$ in different stellar mass bins, for the normal galaxies, and for the radio source host galaxies.

population have different properties, notably in terms of redshift and magnitude distribution. Therefore, in order to reliably compare the infrared properties of these two distinct populations, for each radio source host galaxy we compute the quantity $\Delta^{\rm R}_{\rm IR} - \langle\Delta^{\rm N}_{\rm IR}({\rm d}z, {\rm d}M)\rangle$, where $\Delta^{\rm R}_{\rm IR}$ is the infrared excess of the given radio source host, which is in the mass bin dM and in the redshift bin dz, and $\langle\Delta^{\rm N}_{\rm IR}({\rm d}z, {\rm d}M)\rangle$ is the average value of the infrared excess for the normal galaxies that lie in the same mass and redshift bin. Figure 7 shows that an infrared excess remains observed for the radio source host galaxies with low stellar masses. The high stellar mass radio source hosts do not show an infrared excess. This result is further discussed in Sect. 5.

4. The environment of the host galaxies of radio sources

In order to study the environment of radio sources, we use a scale-dependent estimator of the overdensity around a given galaxy, which is based on the photometric redshift probability functions. The overdensity estimator is described in detail in Appendix A. This estimator has the advantage of (i) having a physical comoving scale as input, (ii) fully using the information contained within the photometric redshift probability function, and (iii) controling edge effects. Overdensities found on large scales may relate to galaxy clusters, whereas smaller scales may relate to small groups of galaxies, or pairs of galaxies.

4.1. The overdensity parameter

The derivation of the overdensity parameter is described fully in Appendix A, but we summarise it here. The $\chi^2(z)$ that were available from ZPEG for all the objects of the CFHTLS-W1 field (Tasse et al. 2008) are first converted into probability functions $p(z)$. Given an object, its associated $p(z)$, and a comoving scale $R_{\rm kpc}$, we estimate the number of objects n enclosed in the cocone of radius $R_{\rm kpc}$. Because the optical survey is flux limited, the estimate of n strongly depends on the probability function of the considered object: if the object is at high redshift, only the most luminous nearby galaxies can be detected, which biases the number density towards lower values. Therefore, we define the overdensity parameter with the significance of a given observed n. To do this, we generate 20 catalogs containing the same objects, with uniformly distributed positions (no clustering). In each of these catalogs, the number density $n_{\rm unif}$ around the given object is calculated and the mean $\langle n_{\rm unif}\rangle$ and standard deviation $\sigma(n_{\rm unif})$ are estimated. The overdensity ρ is then computed as $\rho = (n - \langle n_{\rm unif}\rangle)/\sigma(n_{\rm unif})$.

We have derived the overdensity parameter on 75, 250, and 450 kpc scales for both the radio source host galaxies sample and for the normal galaxies. Figure 8 shows an example of the overdensity parameter estimates derived for the $i < 23$ objects within a $5' \times 5'$ field. We chose this location because it contains galaxies belonging to a galaxy cluster as well as field galaxies. Qualitatively, our algorithm looks efficient: a high overdensity parameter corresponding to an overdense region is seen at the location where the overdensity is obvious in the sky plane.

4.2. The environment of radio sources

The overdensity parameter is likely to be quite sensitive to the mass of the object, and some residual redshift dependence may remain. Comparing the overdensity distributions of two populations having different magnitude and redshift distributions would therefore be misleading. Instead, in the following, we compare the environment of a given radio source host galaxy to that of the normal galaxy population in the same mass and redshift range. We do this by computing the quantity $\Delta\rho_i = \rho_i - q_{0.5}[\rho^{\rm N}({\rm d}z, {\rm d}M)]$, where ρ_i is the overdensity of

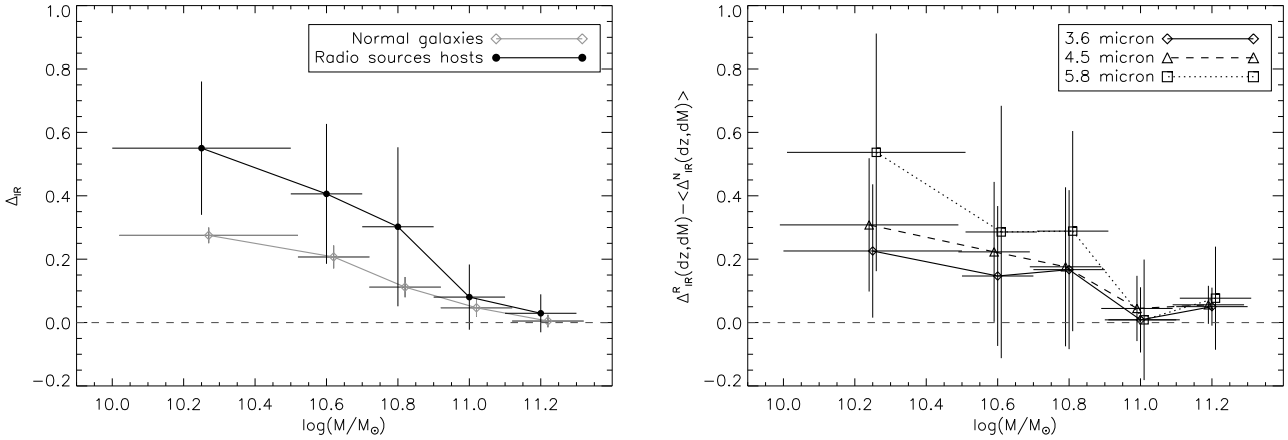

Fig. 7. The *left panel* shows the infrared excess Δ_{IR} at 3.6 μm for the radio source host galaxies and for the normal galaxies. In the *right panel*, we compare the infrared excess of individual radio source host galaxies with normal galaxies that are in the same mass and redshift range.

the given galaxy in the redshift and mass bins (dz, dM), while $\langle\rho^N(dz, dM)\rangle$ $q_{0.5}[\rho^N(dz, dM)]$ is the median overdensity parameter of normal galaxies in the same redshift and stellar mass interval. In practice, dM is taken to be the stellar mass bin, and we set $dz = 0.1$.

Figure 9 shows the median value of $\Delta\rho$ in different stellar mass bins and at different scales. The observed relations were bin dependent, therefore we smooth the observation with a box of width $\Delta M = 0.4$. In order to quantify the uncertainty in the median value estimate, we follow a Monte-Carlo approach. We assume the $\Delta\rho$ distributions have the same shape in all stellar mass bins. By generating samples of n sources following the same distribution we estimate the error bar on the median as the standard deviation between the estimated median and the true median.

A stellar mass dichotomy appears in Fig. 9, with the two different environmental regimes occuring above and below a stellar mass range of $\sim 10^{10.5-10.8}$ $M_\odot$. The higher stellar mass radio source host galaxies lie in a 450 kpc scale environment that is on average denser than the environment of the non-radio-loud galaxies of the same mass by $\Delta(\rho) \sim 0.7$, while their small scale environment has $\Delta(\rho) \sim 0$. An inverse relation is observed for the low stellar masses objects: their small scale 75 kpc scale environment is denser than the average by $\Delta\rho \sim 0.3$, while their large scale environment is significantly underdense on average, with $\Delta\rho \sim -0.5$.

However, the estimated overdensities may be dependent at the different scales: high 450 kpc scale overdensities may lead to higher 75 kpc scale overdensities. In order to study the 75 kpc overdensities of radio source host galaxies independently of their large 450 kpc environment, we compute the quantity $\Delta\rho(75|450) = \rho_{i,75} - q_{0.5}[\rho^N_{75}(dz, dM, d\rho_{450})]$, where $q_{0.5}[\rho^N_{75}(dz, dM, d\rho_{450})]$ is the median overdensity of non-radio-loud galaxies that lie in similar large scale environments and that have comparable stellar mass and redshift estimates. Similarly, we compute $\Delta\rho(450|75)$, and we take $d\rho = 0.3$. Figure 9 shows $\Delta\rho(75|450)$ and $\Delta\rho(450|75)$: the environmental dichotomy remains observed with the stellar mass cut in the range $\sim 10^{10.8-11.0}$ $M_\odot$. These results are further discussed in Sect. 5.

4.3. Comparison with X-ray selected galaxy clusters

In order to provide some quantification of what the values of the overdensity parameters for the radio source hosts actually mean, we take advantage of the XMM X-ray data of the field which provides samples of X-ray groups and clusters. In this section we compare the overdensities found around radio sources to overdensity estimates of X-ray groups and clusters of different bolometric luminosity (i.e. dark matter halo mass), to place further constraints on the environment of radio sources determined in Sect. 4.2.

Here we consider the sample of X-ray clusters detected as extended X-ray emission (Pacaud et al. 2006) in the initial ~5 deg^2 of the XMM-LSS field (Pierre et al. 2004), and were spectroscopically confirmed (Pierre et al. 2006). By fitting a model of free-free emission to the X-ray spectra of 29 sources, Pierre et al. (2006) and Pacaud et al. (2007) measured bolometric luminosities as well as temperatures. Only 12 of those sources overlap with the CFHTLS-W1 field, however, so to increase the size of the X-ray cluster sample we also consider the X-ray sources classified as extended by the X-ray pipeline, but which have not yet been spectroscopically confirmed. The final sample of extended X-ray sources contains 35 sources in the redshift range $z \lesssim 1.2$. We describe below how we derived a crude estimation of the redshifts and bolometric luminosities of these clusters.

We estimated the overdensity on 75, 250 and 450 kpc scales for the galaxies that lie within 30″ of the galaxy clusters detected as extended X-rays sources. In most cases, inspecting the $\rho_{450} - z$ plane showed a peak in the redshift distribution of the galaxies aligned with a given extended X-ray source, and having a high $\rho_{450} > 2$ overdensity estimate. If a redshift peak was detected, we assigned that redshift to the extended X-ray emission, otherwise we rejected the X-ray source. We estimated the bolometric luminosity using the X-ray pipeline XSPEC. We modelled the X-ray emission with a bremsstrahlung emission model (named "APEC" in XPEC), assuming a metal abundance of 0.3 $Z_\odot$, a temperature of 3 keV at each redshift in $0 < z < 2$, and thus derived a [0.5–2] keV flux to bolometric luminosity conversion factor. Based on this estimate of the X-ray luminosity, we estimated the gas temperature by assuming that the clusters of galaxies follow the temperature versus luminosity relation (Arnaud & Evrard 1999). We derived new estimates of the bolometric

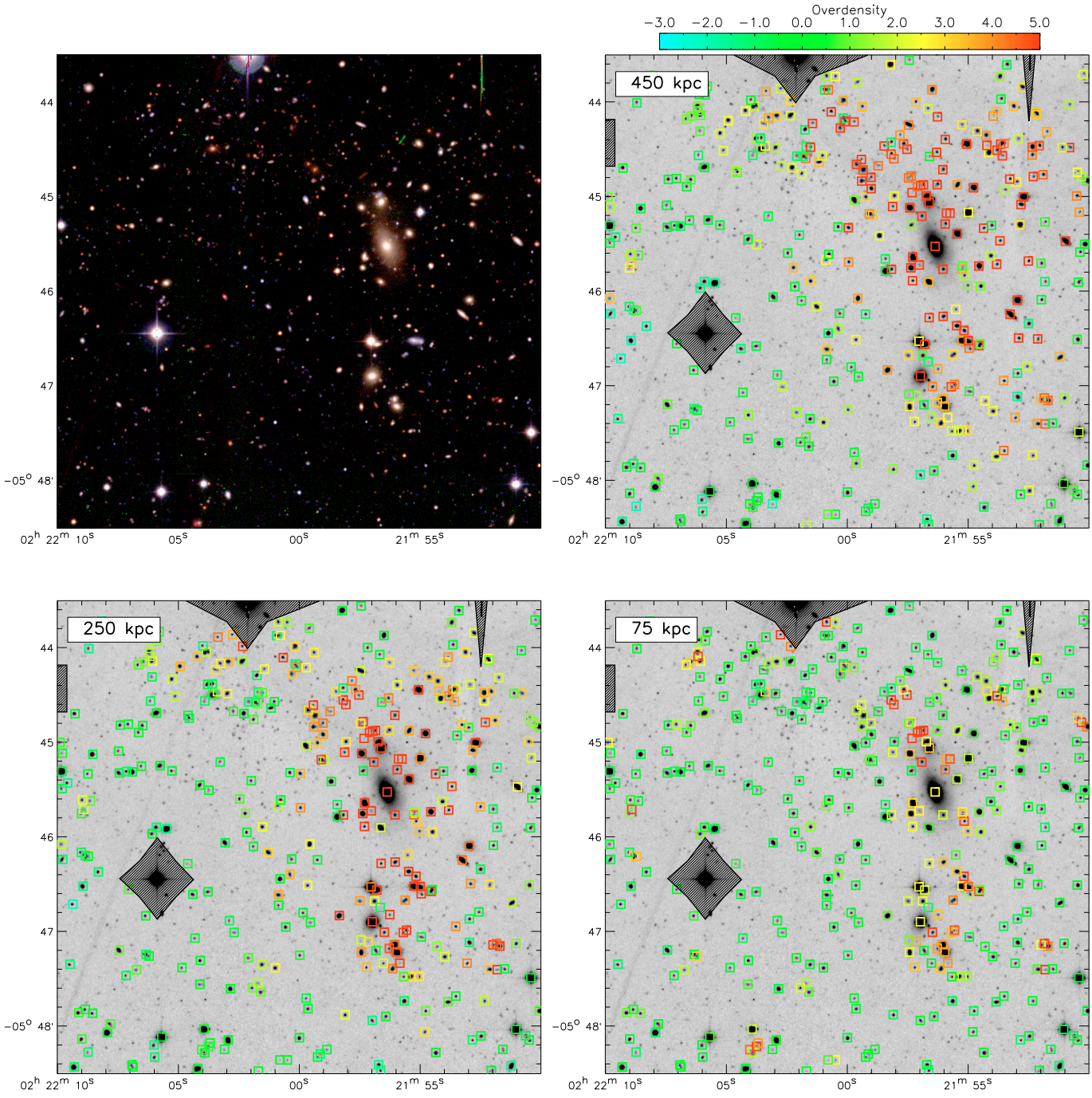

Fig. 8. Overdensity estimator based on the individual photometric redshift probability functions. *Top left panel* shows a given region of the CFHTLS field in which we have computed the overdensity parameter at different scales for the objects brighter than $i = 23$. The other panels show the overdensity for each object on 450, 250 and 75 kpc scales, following the color code of top right panel. The clustering at the different scales is different. The galaxy cluster that appears visually obvious in the i-band image is detected with a 450 kpc scale giving many galaxies an overdensity parameter $\rho_{450} \gtrsim 5$. Decreasing the overdensity scale enhances small groups of galaxies or even galaxy mergers.

luminosity based on these temperature estimates. For the extended X-ray sources confirmed spectroscopically (Pacaud et al. 2007), Fig. 10 shows the comparison between the bolometric luminosities, as estimated using (i) the combination of photometric redshift and overdensity parameter and (ii) the spectroscopic redshifts and spectral fits (Pacaud et al. 2007). Except for one point[2], the two estimates agree within ∼0.2 dex.

Figure 11 shows the averaged values of $\Delta\rho$ (see Sect. 4.1) in different galaxy stellar mass and bolometric luminosity ranges. Galaxies aligned within a luminous X-ray cluster have higher overdensity estimates: in the luminosity range $L_X > 10^{43.5}$ erg s^{-1}, $\Delta\rho$ is as high as ∼9, while $\Delta\rho \sim 3$ at $L_X < 10^{43.0}$ erg s^{-1}. We interpret this effect as being caused by an increase of the *true* overdensity with increasing X-ray luminosity, as it is well known that the bolometric luminosity of the X-ray

[2] Many of the galaxies in this cluster are saturated in the i-band optical image. The redshift that has been associated with this cluster following our method is the photometric redshift of background optical objects aligned with the X-ray cluster. This leads to an incorrect estimate of its X-ray luminosity.

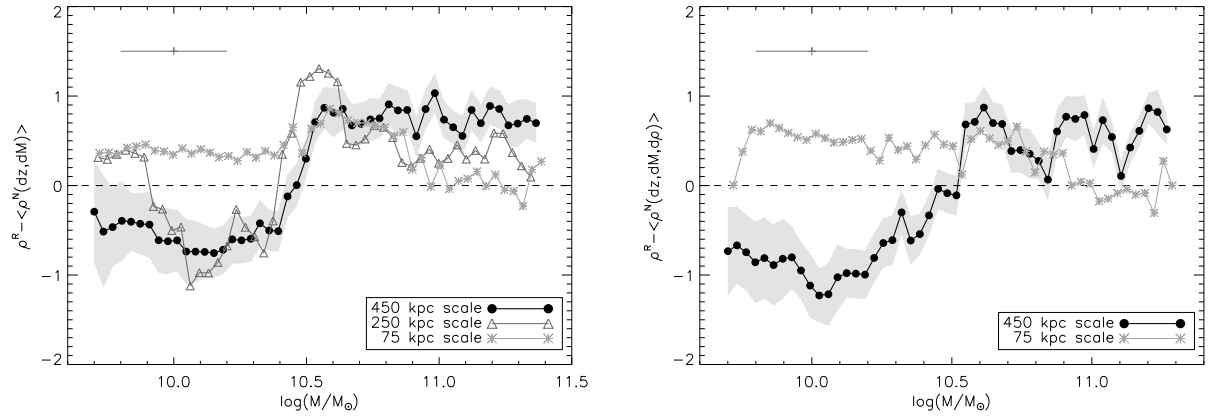

Fig. 9. *Left panel*: the difference in overdensity parameter $\Delta\rho$ between the radio source host galaxies, and the normal galaxies, as a function of the stellar mass. Because these two populations are significantly different in terms of redshift and magnitude distribution notably, we compare the overdensity of each radio source to the overdensity around normal galaxies in the same mass and redshift bin. This quantity is plotted for different input scales. However, the overdensity estimates on a given scale may depend on the overdensity estimate on another scale. In order to address that issue, in the *right panel* we compute the overdensity differences $\Delta\rho$ on small and large scale for galaxies situated in similar large and small scale environments respectively (see discussion in the text). The environmental dichotomy remains observed.

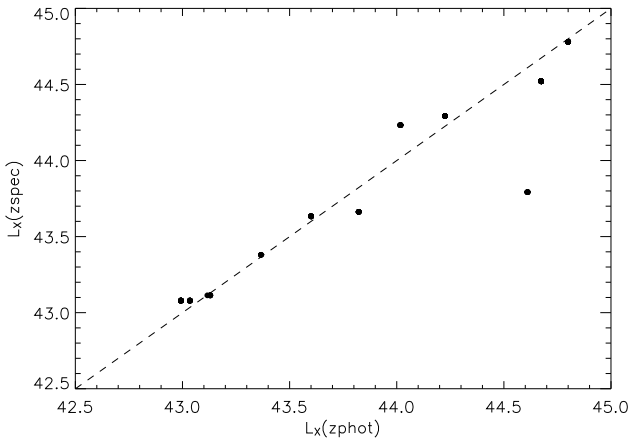

Fig. 10. The comparison between our estimate of the bolometric luminosity (L_X(zphots)) with the bolometric luminosity L_X(zspec) as deduced using spectroscopic redshift and X-ray spectral fits. The two estimates are in reasonable agreement.

emitting gas correlates with the dark matter halo mass (Popesso et al. 2005).

Although the overdensity parameter might be biased by redshift effects, and probes number density rather than mass, it seems we can further constrain the environment of radio sources. We can already see from the overdensity estimates of the galaxies in the brightest ($L_X > 10^{43.5}$ erg s^{-1}) X-ray clusters that, although they have a similar redshift distribution to the radio source host galaxies, their overdensities are far higher. The overdensity around radio sources is similar to or even lower than the overdensity found within the lower luminosity clusters, whose halo masses are of the order of $M \sim 10^{14}$ $M_\odot$ (Popesso et al. 2005). These results are consistent with previous studies in which radio source host galaxies were found to be preferentially located in environments of moderate density (e.g. Hill & Lilly 1991; Best 2000).

5. Discussion and conclusions

In this paper we have carried out a series of analyses giving further evidence that our estimates of photometric redshifts and stellar masses for the host galaxies of the radio source sample built in Tasse et al. (2008) are reliable. Specifically, our estimate of the $V/V_{\rm max}$ vs. radio power relation fits the SDSS measurement of Clewley & Jarvis (2004), suggesting there should be no systematic between the radio luminosity and the accuracies of the photometric redshifts. Also, in the lowest redshift bin $0.1 < z < 0.6$, the relation betweeen the fraction of radio-loud galaxies and the stellar mass relation is in good agreement with the SDSS $z \lesssim 0.3$ measurement in the radio power range $P_{1.4} > 10^{24}$ W Hz^{-1} from Best et al. (2005).

In Sects. 3 and 4, we investigated the intrinsic and environmental properties of radio source host galaxies as compared to the normal galaxy population. The sample extends up to $z \sim 1.2$, and across the 1.4 GHz radio power range 10^{24-27} W Hz^{-1} (see Fig. 1). The main results are as follows:

(i) the relationship between the fraction of radio-loud galaxies and the stellar mass shows a break in the range $M \sim 10^{10.8-11}$ $M_\odot$ and $z \gtrsim 0.5$;
(ii) the low stellar mass radio source host galaxies show a stronger evolution than the high stellar mass galaxies. At $z \sim 1$, the mass function of radio source host galaxies appears to be significantly flatter than in the local universe;
(iii) high stellar mass radio sources are seen to be preferentially located in poor clusters of galaxies;
(iv) the environment of the low stellar mass radio sources is biased towards large-scale underdensities, and small-scale overdensities;
(v) at $M \lesssim 10^{10.8-11}$ $M_\odot$, galaxies have a hot dust component observed as an infrared excess, while the galaxies with $M \gtrsim 10^{10.8-11}$ $M_\odot$ do not.

These results suggest the existence of dichotomy in the nature of both the hosts and environment of radio sources. We argue below that the observed dichotomy might be caused by the different ways of triggering the black hole activity as discussed in Sect. 1.

Best et al. (2005) used a large sample of low luminosity radio sources in the SDSS ($z \lesssim 0.3$) to show that the fraction $f_{\rm RL}$ of radio loud galaxies scales with the galaxy stellar mass as

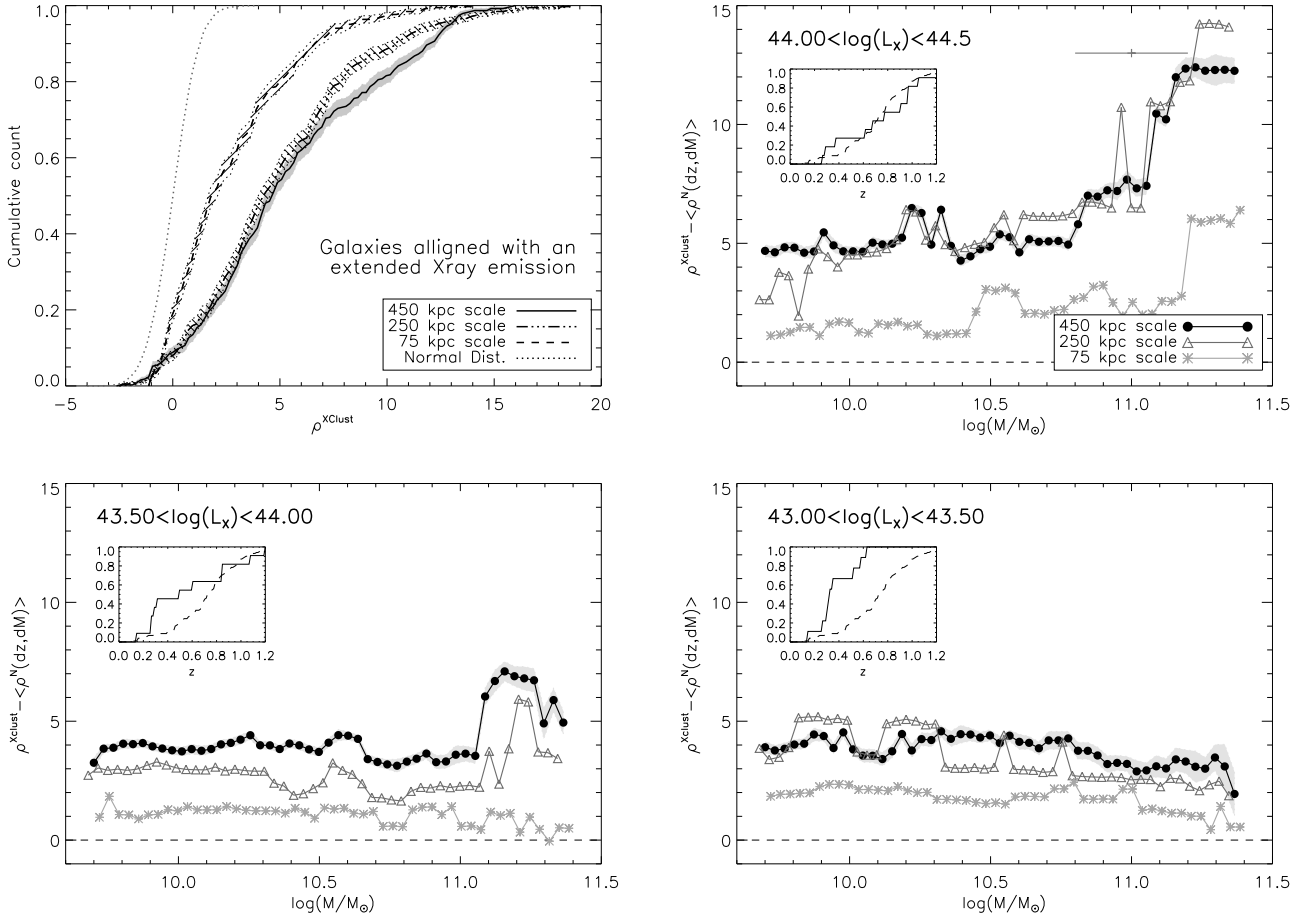

Fig. 11. *Top left panel*: the overdensity parameter for the galaxies aligned with X-ray cluster emission and field galaxies in the same redshift ranges. The overdensity parameter appears to be quite efficient. *Top right to bottom right*: the difference in overdensity parameter between the galaxies aligned with X-ray cluster emission and the field galaxies for different X-ray luminosities. In each panel, the estimated redshift distribution of the X-ray clusters is indicated (full line), and compared to the redshift distribution of the radio source host galaxies (dashed line). Although our overdensity parameter is biased by redshift, it seems that the increase of the halo mass leads to a higher overdensity parameter estimate. Comparing this with Fig. 9, it seems that massive radio sources lie in rather small clusters on average.

$f_{\rm RL} \propto M^{2.5}$, and argued that the IGM gas cooling rate $\dot{M}$ that has the same dependence on stellar mass ($\dot{M}_{\rm cool} \propto M^{2.5}$), providing a way of feeding the black hole and triggering the AGN. For our dataset, in the redshift range $0.1 < z < 0.6$ the fraction of radio loud galaxies show a similar dependence on the stellar masses of galaxies. Furthermore, our result (iii) supports this picture as the high stellar mass systems that are radio-loud are preferentially located in large 450 kpc scale overdense environments as compared to non-radio-loud galaxies of the same mass. This environment resembles small clusters of galaxies with $M \sim 10^{14}\ M_\odot$, in agreement with observations of low redshift radio sources lying in moderate groups to poor clusters (Best 2004, and references therein). In contrast, Best et al. (2007) found that the radio-loud fraction versus stellar mass relation flattens to $f_{\rm RL} \propto M^{1.5}$ for a sample of brightest cluster galaxies (BCGs), while there is evidence that the radio sources observed at high redshift lie in rich cluster environments (Best et al. 2003; Kurk et al. 2004; Venemans 2006). Interestingly, in the redshift bin $0.6 < z < 1.2$, the radio sources with $P_{1.4} > 10^{25}$ W Hz^{-1} show a dependence of $f_{\rm RL}$ with the stellar mass that flattens to $f_{\rm RL} \propto M^{\sim 1.8}$, which could be due to a greater fraction of radio-loud galaxies that are located at the center of galaxy clusters by $z \sim 1$.

Result (iv) suggests that the low stellar mass, strongly evolving component of the radio source host galaxy population inhabit a different environment than the radio-loud AGN with high stellar mass host galaxies discussed above. Compared to normal galaxies of the same mass, radio-loud galaxies preferentially lie in large scale underdensities (450 kpc comoving), and overdensities at small scales (75 kpc), suggesting their AGN activity may be triggered by galaxy mergers and interactions. Similarly, ULIRGs are found to be associated with galaxy interactions or galaxy mergers (Sect. 1), and star forming galaxies have been shown to be preferentially located in underdense environments, where the low velocity dispersion conditions favour galaxy mergers and interactions (Gómez et al. 2003; Best 2004). Furthermore the low mass radio-loud AGN in our sample have a significant infrared excess at 3.6 μm (observer frame) as compared to non-radio-loud galaxies of the same mass. Seymour et al. (2007) have already observed such infrared excesses in powerful high redshift radio galaxies, and concluded that this is due to the presence of hot ($\sim$0.5–1 $\times 10^3$ K) dust, heated by an obscured, highly accreting AGN. This is consistent with AGN unified schemes whereby these objects are radiatively efficient radio-loud quasars viewed edge-on.

As discussed in Hardcastle et al. (2007), the state of the gas that reaches the black hole might play an important role in triggering the quasar and the radio modes (Sect. 1). The observed environmental dichotomy reported here, with the low stellar mass ($M < 10^{11}\ M_\odot$) systems having a hot infrared excess, support the picture in which the galaxy interactions or mergers trigger high efficiency accretion, while the hot gas cooling from the atmosphere of massive galaxies triggers the radiatively inefficient accretion of low luminosity radio-loud AGN. It might be that the number density of low-mass radio-loud AGN is low in the nearby Universe because the combination of a fairly massive black hole and a galaxy merger or interaction that can supply cold gas, are quite rare. However, these conditions will be more common in the gas-rich early Universe, which might explain the higher number density of low stellar mass radio-loud AGN at higher redshift. As the large scale structure forms and the environment of galaxies changes, the two competing mechanisms discussed in this paper may play an important role in the evolution of the AGN activity.

Acknowledgements. The optical images were obtained with MegaPrime/MegaCam, a joint project of CFHT and CEA/DAPNIA, at the CFHT which is operated by the National Research Council (NRC) of Canada, the Institut National des Sciences de l'Univers of the Centre National de la Recherche Scientifique (CNRS) of France and the University of Hawaii. This work is based on data products produced at TERAPIX and at the Canadian Astronomy Data Centre as part of the CFHTLS, a collaborative project of NRC and CNRS.

Appendix A: Overdensity estimator

A.1. Probability functions

The use of photometric redshifts codes is generally limited to the determination of the values associated with the best fitting template, which do not include multiple solutions, for example. In order to fully use the information derived from the fitting of the magnitude points, as described in Tasse et al. (2008), the least χ^2 was recorded as a function of the redshifts for 200 values in $0 < z < 2$. Following Arnouts et al. (2002), for each object, we relate the $\chi^2(z)$ function to the photometric redshift probability function $p(z)$ as follows:

$$p(z) \propto \chi^{r-2}(z) \exp\left(-\chi^2(z)/2\right) \tag{A.1}$$

where r is the number of degrees of freedom. Assuming that all optical sources have their true redshift in $0 < z < 2$, $\int p(z)\mathrm{d}z$ is normalized to 1 over this redshift interval.

A.2. Overdensity parameter

In order to build our overdensity parameter, we calculate the mean number density around a chosen galaxy within an arbitrary chosen comoving volume, using the information contained in the probability function $p(z)$.

A radius $R_{\rm kpc}$ is first chosen in the comoving space. It defines a comoving scale to which the overdensity estimate refers. Overdensities over large scales may refer to galaxy clusters, whereas smaller scales may refer to small groups of galaxies or even galaxy pairs.

The redshift space is then binned so that the volume V of the cone of radius $R_{\rm kpc}$ and line-of-sight comoving length $D_{\rm c}(\Delta z_i)$ stays constant. We choose V so that $\Delta z_i = z_{i+1} - z_i \approx 0.1$, the typical error bar on photometric redshifts (Tasse et al. 2008). This leads to $z_i = \{0.05, 0.12, 0.19, 0.28, 0.38, 0.49, 0.62, 0.76, 0.92, 1.10, 1.29\}$. In each redshift bin i centered at $(z_i + z_{i+1})/2$, the angular diameter $R_{\rm i,deg}$ corresponding to $R_{\rm kpc}$ is calculated. Then, we derive the density around the given object inside each redshift slice:

$$n_i = f_{\rm eff} \sum_{j \in \Omega_i} \left(\int_{z_i}^{z_{i+1}} p_j(z)\mathrm{d}z \right) \tag{A.2}$$

where Ω_i is the set of the objects found within $R_{\rm i,deg}$ around the considered objects, and $f_{\rm eff}$ is a term designed to correct for edges effects, for example, when the circle of diameter $R_{i,\rm deg}$ overlaps with a masking region or the edges of the field. In that case, we make the assumption that the number density of sources within the masked area is the same as the unmasked area within $R_{i,\rm deg}$. We then have $f_{\rm eff} = \pi R^2_{i,\rm deg}/(\pi R^2_{i,\rm deg} - A_{\rm masked})$, with $A_{\rm masked}$ being the masked area. Then, the mean density around the considered source can be written as:

$$n = \sum_i \left(n_i \int_{z_i}^{z_{i+1}} p(z)\mathrm{d}z \right) \tag{A.3}$$

where $p(z)$ is the probability function of the considered object. The estimate of n greatly depends upon the given object probability function. In order to quantify the significance of the number density estimate around the given object with a given probability function, we determine the mean and standard deviation of n (Eq. (A.3)) in a similar catalog but in the absence of clustering. In practice, we extract a catalog in a $0.2^\circ \times 0.2^\circ$ square around the source in the CFHTLS-Wide catalog, and reassign each object a uniformly distributed random position. We make 20 realisations of such a catalog, and in each we derive the number density $n_{\rm unif}$ around the considered objects using Eqs. (A.2) and (A.3). We compute the mean $\langle n_{\rm unif}\rangle$ and the standard deviation $\sigma(n_{\rm unif})$ of the number density around the considered object when there is no clustering. The overdensity is finally defined as $\rho_{\rm sc} = (n - \langle n_{\rm unif}\rangle)/\sigma(n_{\rm unif})$, giving us the significance of the number density estimate.

References

Arnaud, M., & Evrard, A. E. 1999, MNRAS, 305, 631
Arnouts, S., Moscardini, L., Vanzella, E., et al. 2002, MNRAS, 329, 355
Avni, Y., & Bahcall, N. A. 1976, ApJ, 209, 16
Avni, Y., & Bahcall, J. N. 1980, ApJ, 235, 694
Best, P. N. 2000, MNRAS, 317, 720
Best, P. N. 2004, MNRAS, 351, 70
Best, P. N., Lehnert, M. D., Miley, G. K., & Röttgering, H. J. A. 2003, MNRAS, 343, 1
Best, P. N., Kauffmann, G., Heckman, T. M., et al. 2005, MNRAS, 362, 25
Best, P. N., Kaiser, C. R., Heckman, T. M., & Kauffmann, G. 2006, MNRAS, 368, L67
Best, P. N., von der Linden, A., Kauffmann, G., Heckman, T. M., & Kaiser, C. R. 2007, MNRAS, 527
Clewley, L., & Jarvis, M. J. 2004, MNRAS, 352, 909
Condon, J. J., Cotton, W. D., Greisen, E. W., et al. 1998, AJ, 115, 1693
Croton, D. J., Farrar, G. R., Norberg, P., et al. 2005, MNRAS, 356, 1155
Croton, D. J., Springel, V., White, S. D. M., et al. 2006, MNRAS, 365, 11
Dunlop, J. S., & Peacock, J. A. 1990, MNRAS, 247, 19
Elitzur, M. 2007, ASP Conf. Ser. 373, ed. L. C. Ho, & J.-W. Wang, 415
Evans, D. A., Worrall, D. M., Hardcastle, M. J., Kraft, R. P., & Birkinshaw, M. 2006, ApJ, 642, 96
Fontana, A., Pozzetti, L., Donnarumma, I., et al. 2004, A&A, 424, 23
Fontana, A., Salimbeni, S., Grazian, A., et al. 2006, A&A, 459, 745
Gebhardt, K., Bender, R., Bower, G., et al. 2000, ApJ, 539, L13
Gómez, P. L., Nichol, R. C., Miller, C. J., et al. 2003, ApJ, 584, 210
Hardcastle, M. J., Evans, D. A., & Croston, J. H. 2006, MNRAS, 370, 1893
Hardcastle, M. J., Evans, D. A., & Croston, J. H. 2007, MNRAS, 376, 1849
Hill, G. J., & Lilly, S. J. 1991, ApJ, 367, 1
Hine, R. G., & Longair, M. S. 1979, MNRAS, 188, 111
Jackson, N., & Rawlings, S. 1997, MNRAS, 286, 241
Kauffmann, G., Heckman, T. M., Tremonti, C., et al. 2003, MNRAS, 346, 1055

Kurk, J. D., Pentericci, L., Overzier, R. A., Röttgering, H. J. A., & Miley, G. K. 2004, A&A, 428, 817
Laing, R. A., Jenkins, C. R., Wall, J. V., & Unger, S. W. 1994, in The Physics of Active Galaxies, ed. G. V. Bicknell, M. A. Dopita, & P. J. Quinn, ASP Conf. Ser. 54, 201
Le Borgne, D., & Rocca-Volmerange, B. 2002, A&A, 386, 446
Lonsdale, C. J., Smith, H. E., Rowan-Robinson, M., et al. 2003, PASP, 115, 897
Mathews, W. G., & Brighenti, F. 2003, ARA&A, 41, 191
Ogle, P., Whysong, D., & Antonucci, R. 2006, ApJ, 647, 161
Pacaud, F., Pierre, M., Refregier, A., et al. 2006, MNRAS, 372, 578
Pacaud, F., Pierre, M., Adami, C., et al. 2007, MNRAS, in prep.
Pierre, M., Valtchanov, I., Altieri, B., et al. 2004, J. Cosmology Astro-Particle Phys., 9, 11
Pierre, M., Pacaud, F., Duc, P.-A., et al. 2006, MNRAS, 372, 591
Popesso, P., Biviano, A., Böhringer, H., Romaniello, M., & Voges, W. 2005, A&A, 433, 431
Sanders, D. B., & Mirabel, I. F. 1996, ARA&A, 34, 749
Sanders, D. B., Soifer, B. T., Elias, J. H., et al. 1988a, ApJ, 325, 74
Sanders, D. B., Soifer, B. T., Elias, J. H., Neugebauer, G., & Matthews, K. 1988b, ApJ, 328, L35
Schmidt, M. 1968, ApJ, 151, 393
Schmitt, H. R. 2004, in The Interplay Among Black Holes, Stars and ISM in Galactic Nuclei, ed. T. Storchi-Bergmann, L. C. Ho, & H. R. Schmitt, IAU Symp., 222, 395
Seymour, N., Stern, D., De Breuck, C., et al. 2007, ApJS, 171, 353
Snellen, I. A. G., & Best, P. N. 2001, MNRAS, 328, 897
Springel, V., Di Matteo, T., & Hernquist, L. 2005a, ApJ, 620, L79
Springel, V., Di Matteo, T., & Hernquist, L. 2005b, MNRAS, 361, 776
Sutherland, W., & Saunders, W. 1992, MNRAS, 259, 413
Tasse, C., Cohen, A. S., Röttgering, H. J. A., et al. 2006, A&A, 456, 791
Tasse, C., Le Borgne, D., Röttgering, H. J. A., et al. 2008, A&A, 490, 879
Tasse, C., Röttgering, H. J. A., Best, P. N., et al. 2007, A&A, 471, 1105
Veilleux, S. 2003, in Active Galactic Nuclei: From Central Engine to Host Galaxy, ed. S. Collin, F. Combes, & I. Shlosman ASP Conf. Ser., 290, 11
Venemans, B. P. 2006, Astron. Nachr. 327, 196
Whysong, D., & Antonucci, R. 2004, ApJ, 602, 116
Willott, C. J., Rawlings, S., Blundell, K. M., Lacy, M., & Eales, S. A. 2001, MNRAS, 322, 536